A MEMS-based Adaptive AHRS for Marine Satellite Tracking Antenna

Wang, Yunlong; Hussain, Dil muhammed Akbar; N. Soltani, Mohsen

Published in:
IFAC-PapersOnLine

DOI (link to publication from Publisher):
10.1016/j.ifacol.2015.10.268

Publication date:
2015

A MEMS-based Adaptive AHRS for Marine Satellite Tracking Antenna ⋆

Yunlong Wang *, **Akbar Hussain** *, **Mohsen Soltani** *

* *Department of Energy Technology, Aalborg University, Esbjerg 6700, Denmark (e-mail: way@et.aau.dk, akh@et.aau.dk, sms@et.aau.dk).*

Abstract: Satellite tracking is a challenging task for marine applications. An attitude determination system should estimate the wave disturbances on the ship body accurately. To achieve this, an Attitude Heading Reference System (AHRS) based on Micro-Electro-Mechanical Systems (MEMS) sensors, composed of three-axis gyroscope, accelerometer and magnetometer, is developed for Marine Satellite Tracking Antenna (MSTA). In this paper, the attitude determination algorithm is improved using an adaptive mechanism that tunes the attitude estimator parameters based on an estimation of ship motion frequency. In order to get fast running cycle frequency of attitude estimator, Kalman filter is simplified to reduce calculation burden together with other improvemetns. An Immersion and Invariance (I&I) frequency estimator is designed using Lyapunov theory to estimate the ship motion frequency. The estimated frequency is then used to adjust the gain matrix in Kalman filter. The designed algorithms are implemented in ARM processor and the attitude obtained is compared to a high-precision commercial Inertial Measurement Unit (IMU) to validate the performance of designed AHRS.

Keywords: AHRS, attitude estimation, Immersion and Invariance frequency estimator.

1. INTRODUCTION

Marine Satellite Tracking Antenna (MSTA) is an essential component for the satellite communication with ships and vessels. In order to maintain the communication link, the antenna line of sight has to be directed toward the satellite. This is not a difficult task when the antenna is used on a static platform. Once the antenna is mounted on ships, which would sway heavily during heavy sea states, a high-precision attitude control system is needed to stabilize the antenna to obtain a tracking error of less than a fraction of a degree. In this system, high accuracy attitude measurement is a key issue.

Up until the present time, most MSTAs use rate gyro sensors and beam sensor to achieve attitude control (Soltani (2008); Soltani et al. (2011, 2008); Tseng and Teo (1998)). The angle rates from three rate gyro sensors are integrated separately to get roll, pitch and yaw of antenna dish. Then beam sensor is used to get pointing error feedback for control system to correct the drift angle caused by rate gyro sensors. Others use rate gyro sensor and inclinometer in the antenna control system (Ming et al. (2005)). Meanwhile, most of the previous antenna attitude measurements are based on two axes, that is, azimuth axis and elevation axis.

In this work, MEMS sensors are chosen for attitude determination of the antenna. The advantages of MEMS sensors are their low cost, small size, which are ideal to be used in commercial MSTA to achieve attitude estimation. It is worthwhile trying to use MEMS sensors, such as gyroscope, acceleromter and magnetometer, for getting the attitude of MSTA. However, due to low precision and drift, MEMS gyroscopes alone could not provide useful attitude information, which means they have to be used together with MEMS accelerometer and magnetometer.

In previous researches, some kinds of MEMS-based AHRSs were developed for wearable inertial movement tracking by Madgwick et al. (2011) and Comotti et al. (2013). A MEMS-based AHRS was designed and used for posture control of robot fish by Hu et al. (2013). Chan et al. (2011) applied MEMS-based AHRS in quadrotor control system and Kalman filter is used as sensor data fusion algorithm . Ryan and Miller (2010) used an adaptive bias estimation algorithm in MEMS-based AHRS for pan and tilt surveillance platform. The running cycle frequency of previous MEMS-based AHRSs are relatively low, among which the highest cycle frequency is 200Hz and the lowest one is only 50Hz. Moreover, the estimation errors of attitude angle previous AHRSs during dynamic stage are usually more than 1.5deg, which can not satisfy the requirements of MSTA system.

In the present study, an Attitude Heading Reference System (AHRS) was designed and manufactured to obtain the attitude of MSTA by using MEMS sensors, with cycle frequency of 500Hz. The attitude estimation algorithm is optimized to reduce calculation burden for running in ARM chip. Inspired by Liu et al. (2009), an Immersion and Invariance (I&I) frequency estimator is designed using Lyapunov theory to estimate the ship motion frequency. This algorithm is beneficial as it does not require high computational power. In addition, its convergence is proven. The estimated frequency is then used to adjust the Kalman

⋆ This work was supported by Innovation Fund Denmark under the proojeet STAR^2 COM (Jnr.060-2013-3).

gain matrix resulting in more accurate estimates during during high sea states.

This paper is organized as follows: In Section 2, an attitude estimator in AHRS is introduced. In Section 3, the procedure of designing an I&I frequency estimator is explained with detailed convergence deduction. The hardware platforms that are used to run designed algorithm and the experiment results are presented in Section 4. Section 5 gives the conclusion and discussses future work.

2. ATTITUDE ESTIMATOR IN AHRS

The attitude estimator used in AHRS is a combined Gauss-Newton method and Kalman filter (Madgwick et al. (2011), Comotti et al. (2013)) whose schematic diagram is shown in Fig. 1.

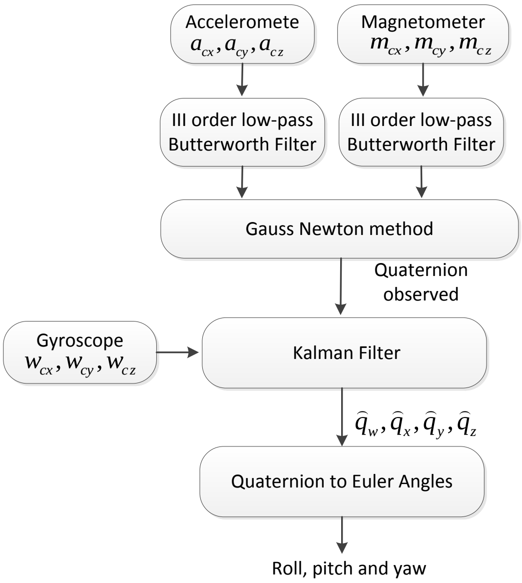

Fig. 1. Schematic diagram of sensor data fusion algorithm.

In Fig. 1, $[w_{cx}, w_{cy}, w_{cz}]$ are calibrated measurements of gyroscope,$[a_{cx}, a_{cy}, a_{cz}]$ are calibrated measurements of acceleromter and $[m_{cx}, m_{cy}, m_{cz}]$ are calibrated measurements of magnetometer. Third-order low-pass Butterworth filter is used to remove high-frequency noise in measurements of acceleromter and magnetometer. Gauss-Newton method is used to get observed quaternion which is then used together with measurements of gyroscope in Kalman filter to get the final estimated quaternion $[\hat{q}_w, \hat{q}_x, \hat{q}_y, \hat{q}_z]$.

In attitude estimator, the state vector is a quaternion $\boldsymbol{x} = [q_w, q_x, q_y, q_z]^T$.

The following notations are used:

- $\bar{\boldsymbol{x}}(k+1)$ is the predicted quaternion at time $k+1$ by means of the estimated quaternion at time k;
- $\hat{\boldsymbol{x}}(k)$ is the estimated quaternion at time k from Kalman filter;
- $\boldsymbol{y}(k)$ is the observed quaternion at time k and is defined as $[q_{wo}, q_{xo}, q_{yo}, q_{zo}]^T$.

The initial state of $\boldsymbol{x}$ can be set as $[1, 0, 0, 0]^T$. Otherwise, the initial state can be calculated from the initial measurements of acceleromter and magnetometer (Wang et al. (2004). The former method is used here.

2.1 Quaternion update equation

The quaternion update equation, also known as state update equation in Kalman filter, is achieved by integration of quaternion derivation using Euler method. The quaternion derivation is expressed as (Comotti (2011))

$$\dot{\boldsymbol{x}} = \frac{1}{2} \cdot \boldsymbol{x} \otimes \boldsymbol{w} \tag{1}$$

$$= \frac{1}{2} \cdot \begin{bmatrix} -q_x \cdot w_{cx} - q_y \cdot w_{cy} - q_z \cdot w_{cz} \\ q_w \cdot w_{cx} + q_y \cdot w_{cz} - q_z \cdot w_{cy} \\ q_w \cdot w_{cy} + q_z \cdot w_{cx} - q_x \cdot w_z \\ q_w \cdot w_{cz} + q_x \cdot w_{cy} - q_y \cdot w_{cx} \end{bmatrix} \tag{2}$$

where $\boldsymbol{w} = [0, w_{cx}, w_{cy}, w_{cz}]^T$ is the angular rate vector from gyroscope.

The equation of Euler method used to update state is expressed as

$$\boldsymbol{x}(k+1) = \boldsymbol{x}(k) + \dot{\boldsymbol{x}} \cdot \delta t \tag{3}$$
$$= \boldsymbol{F} \cdot \boldsymbol{x}$$

where,

$$F = \begin{bmatrix} 1 & -\frac{\delta t}{2} \cdot w_{cx} & -\frac{\delta t}{2} \cdot w_{cy} & -\frac{\delta t}{2} \cdot w_{cz} \\ \frac{\delta t}{2} \cdot w_{cx} & 1 & \frac{\delta t}{2} \cdot w_{cz} & -\frac{\delta t}{2} \cdot w_{cy} \\ \frac{\delta t}{2} \cdot w_{cy} & -\frac{\delta t}{2} \cdot w_{cz} & 1 & \frac{\delta t}{2} \cdot w_{cx} \\ \frac{\delta t}{2} \cdot w_{cz} & \frac{\delta t}{2} \cdot w_{cy} & -\frac{\delta t}{2} \cdot w_{cx} & 1 \end{bmatrix}$$

and δt is sampling period.

2.2 Observed quaternion

The observed quaternion is obtained by minimizing the second norm of the output estimation error given by (Comotti (2011),Comotti et al. (2013))

$$\boldsymbol{e}(\boldsymbol{y}) = \begin{bmatrix} \boldsymbol{a}_0 - \boldsymbol{R}_t \cdot \boldsymbol{a}_t \\ \boldsymbol{m}_0 - \boldsymbol{R}_t \cdot \boldsymbol{m}_t \end{bmatrix} \tag{4}$$

where $\boldsymbol{a}_0$ is the reference vector of the acceleration. $\boldsymbol{m}_0$ is the reference vector of the Earth's magnetic field. The exact values of $\boldsymbol{a}_0$ and $\boldsymbol{m}_0$ will be explained in the following. $\boldsymbol{a}_t$ is the measurement vector of the acceleration. $\boldsymbol{m}_t$ is the measured magnetic field. $\boldsymbol{R}_t$ is Direction Cosine Matrix(DCM) at current time and is expressed as

$$\boldsymbol{R}_t = \begin{bmatrix} \hat{q}_w^2 + \hat{q}_x^2 - \hat{q}_y^2 - \hat{q}_z^2 & 2(\hat{q}_x \cdot \hat{q}_y - \hat{q}_z \cdot \hat{q}_w) & 2(\hat{q}_x \cdot \hat{q}_z + \hat{q}_y \cdot \hat{q}_w) \\ 2(\hat{q}_x \cdot \hat{q}_y + \hat{q}_z \cdot \hat{q}_w) & \hat{q}_w^2 - \hat{q}_x^2 + \hat{q}_y^2 - \hat{q}_z^2 & 2(\hat{q}_y \cdot \hat{q}_z - \hat{q}_x \cdot \hat{q}_w) \\ 2(\hat{q}_x \cdot \hat{q}_z - \hat{q}_y \cdot \hat{q}_w) & 2(\hat{q}_y \cdot \hat{q}_z + \hat{q}_x \cdot \hat{q}_w) & \hat{q}_w^2 - \hat{q}_x^2 - \hat{q}_y^2 + \hat{q}_z^2 \end{bmatrix} \tag{5}$$

where, $[\hat{q}_w, \hat{q}_x, \hat{q}_y, \hat{q}_z]$ are latest estimated quaternion from Kalman filter.

The reference values, $\boldsymbol{a}_0$ and $\boldsymbol{m}_0$, are the normalized values of measurements of accelerometer and magnetometer respectively when AHRS is in zero orientation as defined in Fig. 2, where

- the z axis of designed AHRS is the same as the reverse direction of gravity.
- the plane defined by x, y axis of AHRS is the same as the plane where the the second decomposed component of earth magnetic field, My, is zero.

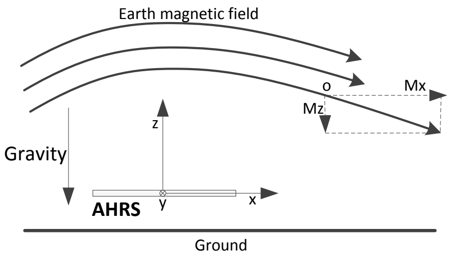

Fig. 2. Schematic diagram of zero orientation of designed AHRS.

Then, the exact values of $\boldsymbol{a}_0$ and $\boldsymbol{m}_0$ are

$$\boldsymbol{a}_0 = [0, 0, -1], \boldsymbol{m}_0 = [\frac{m_{x0}}{\sqrt{m_{x0}^2+m_{z0}^2}}, 0, \frac{m_{z0}}{\sqrt{m_{x0}^2+m_{z0}^2}}]$$

where m_{x0}, m_{z0}, are measurements of magnetometer when AHRS is in zero oritentation.

To minimize (4), Gauss-Newton method is used and is expressed as

$$\boldsymbol{y}(k+1) = \boldsymbol{y}(k) - [\boldsymbol{J}_k^T \cdot \boldsymbol{J}_k]^{-1} \cdot \boldsymbol{J}_k^T \cdot \boldsymbol{e}(\boldsymbol{y}(k)) \qquad (6)$$

where $\boldsymbol{J}_k$ is the Jacobian matrix of $\boldsymbol{e}(\boldsymbol{y}(k))$ (Comotti (2011)).

2.3 Discrete Kalman Filter

When the quaternion update equations and observed quaternions are obtained, discrete-time Kalman filter (Fossen (2011)) will be used here as data fusion algorithm to get estimated attitude.

The design matrices are:

$$\boldsymbol{Q}(k) = \boldsymbol{Q}^T(k) > 0, \boldsymbol{R}(k) = \boldsymbol{R}^T(k) > 0, \bar{\boldsymbol{x}}(0) = \boldsymbol{x}_0$$

where $\boldsymbol{Q}(k)$ and $\boldsymbol{R}(k)$ are usually obtained by calculating the covariance matrices of noise from the measurement of sensors when they are in static state. covariance matrices of noise are usually diagonal matrix. $\boldsymbol{x}_0 = [1, 0, 0, 0]^T$ and is stated at the beginning of Section 2.

The initial error covariance matrix is

$$\bar{\boldsymbol{P}}(0) = diag([1\ 1\ 1\ 1])$$

The Kalman gain matrix is

$$\boldsymbol{K}(k) = \bar{\boldsymbol{P}}(k)\boldsymbol{H}^T(k)[\boldsymbol{H}(k)\bar{\boldsymbol{P}}(k)\boldsymbol{H}^T(k) + \boldsymbol{R}(k)]^{-1} \qquad (7)$$

The State estimate update is

$$\hat{\boldsymbol{x}}(k) = \bar{\boldsymbol{x}}(k) + \boldsymbol{K}(k)[\boldsymbol{y}(k) - \boldsymbol{H}(k)\bar{\boldsymbol{x}}(k)] \qquad (8)$$

The error covariance update is

$$\begin{aligned}\hat{\boldsymbol{P}}(k) = [\boldsymbol{I} - \boldsymbol{K}(k)\boldsymbol{H}(k)]\bar{\boldsymbol{P}}(k)[\boldsymbol{I} - \boldsymbol{K}(k)\boldsymbol{H}(k)]^T \\ +\boldsymbol{K}(k)\boldsymbol{R}(k)K^T(k), \hat{\boldsymbol{P}}(k) = \hat{\boldsymbol{P}}(k)^T > 0\end{aligned} \qquad (9)$$

The state estimation propagation is

$$\bar{\boldsymbol{x}}(k+1) = \boldsymbol{\Phi}(k)\hat{\boldsymbol{x}}(k) + \boldsymbol{\Delta}(k)\boldsymbol{u}(k) \qquad (10)$$

The error covariance propagation is

$$\bar{\boldsymbol{P}}(k+1) = \boldsymbol{\Phi}(k)\hat{\boldsymbol{P}}(k)\boldsymbol{\Phi}^T(k) + \boldsymbol{\Gamma}(k)\boldsymbol{Q}(k)\boldsymbol{\Gamma}^T(k) \qquad (11)$$

Equation (8) to (11) are standard discrete-time Kalman filter. However, a simplified discrete-time Kalman filter, which will be explained in the following, is used here in order to reduce computation burden. In order to get better estimation results, the running cycle of estimator should be as high as possible. By using high running cycle, a smaller step size will be used in integration of gyroscope data and a higher sampling frequency will be applied to get data from sensors, all of which can reduce estimation errors.

When $\boldsymbol{Q}$ and $\boldsymbol{R}$ are set to be constant matrices, the Kalman gain matrix $\boldsymbol{K}$ will converge to a constant matrix after some iterations. The convergence of one element in $\boldsymbol{K}$ can be seen in Fig. 3.

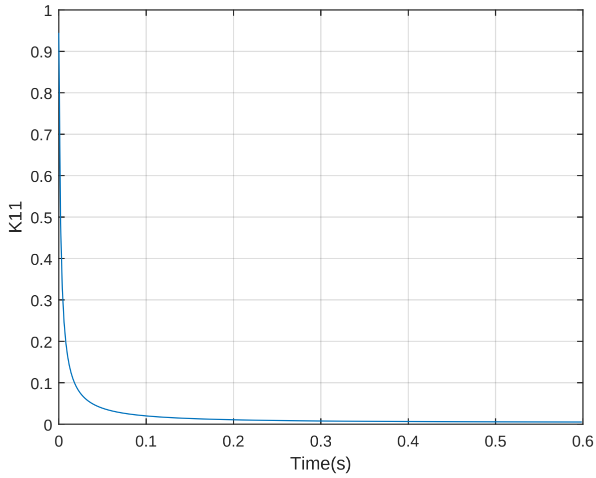

Fig. 3. Convergence of one element in $\boldsymbol{K}$ matrix.

All other elements in $\boldsymbol{K}$ have the same convergence rates as $\boldsymbol{K}_{11}$ in Fig. 3.

A simplified Kalman filter is designed according to the fact that $\boldsymbol{K}$ will converge to a constant matrix. A constant matrix $\boldsymbol{K}_{cst}$ is used directly in (8), as show in (12). Through this method, (9) to (11) do not need to be calculated in each algorithm cycle.

$$\hat{\boldsymbol{x}}(k) = \bar{\boldsymbol{x}}(k) + \boldsymbol{K}_{cst}[\boldsymbol{y}(k) - \boldsymbol{H}(k)\bar{\boldsymbol{x}}(k)] \qquad (12)$$

Then, the calculation burden is largely reduced, which is suitable for implementation in a smaller microprocessor, such as ARM. Moreover, the estimation precision is not affected, which can be seen in Fig. 4.

The $\boldsymbol{K}_{cst}$ can be adjusted if the working condition of designed AHRS changes.

Euler angles can be obtained by (Fossen (2011))

$$\phi = atan2(2(\hat{q}_y \cdot \hat{q}_z + \hat{q}_x \cdot \hat{q}_w), \hat{q}_w^2 + \hat{q}_z^2 - \hat{q}_y^2 - \hat{q}_x^2)$$

$$\theta = -tan^{-1}(\frac{2(\hat{q}_x \cdot \hat{q}_z - \hat{q}_y \cdot \hat{q}_w)}{\sqrt{1 - 2(\hat{q}_x \cdot \hat{q}_z - \hat{q}_y \cdot \hat{q}_w)^2}})$$

$$\psi = atan2(2(\hat{q}_x \cdot \hat{q}_y + \hat{q}_z \cdot \hat{q}_w), \hat{q}_w^2 + \hat{q}_x^2 - \hat{q}_y^2 - \hat{q}_z^2)$$

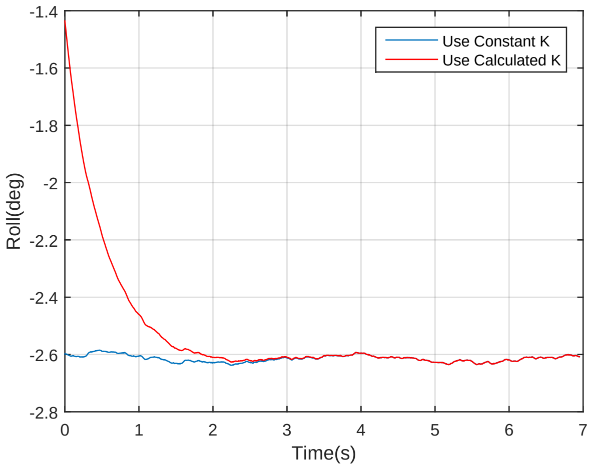

Fig. 4. Comparision of Roll between Kalman filter with calculated $\boldsymbol{K}$ and $\boldsymbol{K}_{constant}$.

where $\hat{q}_w, \hat{q}_x, \hat{q}_y$, and $\hat{q}_z$ are elements of latest estimated quaternion from discrete-time Kalman filter. ϕ, θ, ψ are the roll, pitch, and yaw respectively.

3. I&I FREQUENCY ESTIMATOR

In order to make designed AHRS have good estimation performance under different working environments, an adaptive gain scheduling mechanism is introduced. This mechanism uses the frequency estimations in order to tune the Kalman gain matrix that is tuned off-line for different ship motion frequencies. The main reason for choosing this mechanism is that the weighting matrices R and Q will determine the emphasis on the measurements of the gyros and accelerometers. Introducing a scaling $0 < \gamma(\alpha) < 1$ to these matrices, we have the new Q and R matrices as $Q(\alpha) = \gamma(\alpha)Q$ and $R(\alpha) = (1 - \gamma(\alpha))R$, where α is the highest frequency in pitch and roll rotations. In order to estimate rotation frequency, a fast-converging nonlinear parameter estimator using Inversion and Invariance (I&I) approach is introduced. The I&I estimator is practically feasible for implementation in the ARM processor as it demands a very low computational power. The I&I estimator is inspired by the I&I identification technique of Liu et al. (2009). For the nonlinear system

$$\dot{\boldsymbol{x}} = \boldsymbol{f}(\boldsymbol{x}, \boldsymbol{u}, t) + \boldsymbol{\Phi}(\boldsymbol{x}, \boldsymbol{\alpha}), \tag{13}$$

where $\boldsymbol{x} \in \mathbb{R}^n$, $\boldsymbol{u} \in \mathbb{R}^m$, and $\boldsymbol{\alpha} \in \mathbb{R}^q$ are the states, inputs and constant unknown parameters respectively. The I&I estimator is of the form

$$\begin{aligned} \dot{\hat{\boldsymbol{\xi}}} &= -\frac{\partial \boldsymbol{\ell}(\boldsymbol{x})}{\partial \boldsymbol{x}}[\boldsymbol{f}(\boldsymbol{x}, \boldsymbol{u}, t) + \boldsymbol{\Phi}(\boldsymbol{x}, \hat{\boldsymbol{\xi}} + \boldsymbol{\ell}(\boldsymbol{x}))], \\ \hat{\boldsymbol{\alpha}} &= \hat{\boldsymbol{\xi}} + \boldsymbol{\ell}(\boldsymbol{x}) \end{aligned} \tag{14}$$

under the following two conditions:

(1) There exists $\Omega \subseteq \mathbb{R}^n$ such that $\boldsymbol{\ell} : \Omega \longrightarrow \mathbb{R}^q$ is a smooth mapping.
(2) The mapping

$$\begin{aligned} \boldsymbol{\psi}_{\boldsymbol{x}} &: \mathbb{R}^q \longrightarrow \mathbb{R}^q \\ \boldsymbol{\psi}_{\boldsymbol{x}}(\boldsymbol{\alpha}) &:= \frac{\partial \boldsymbol{\ell}(\boldsymbol{x})}{\partial \boldsymbol{x}} \boldsymbol{\Phi}(\boldsymbol{x}, \boldsymbol{\alpha}) \end{aligned} \tag{15}$$

is strictly monotonically increasing.

In Liu et al. (2010, 2009), conditions are given to ensure that the I&I estimator is asymptotically consistent, i.e., $\lim_{t\to\infty} \hat{\boldsymbol{\alpha}}(t) = \boldsymbol{\alpha}, \ \forall(\boldsymbol{x}(0), \hat{\boldsymbol{\xi}}(0)) \in \Omega \times \mathbb{R}^q \wedge \forall \boldsymbol{u}(t)$.

The I&I estimator is implemented to determine the frequency of the ship motion that is assumed to be a sinusoid or sum of several sine waves (Fossen (2011)). In this case, the ship motion dynamics can be explained by an exosystem with

$$\dot{\boldsymbol{x}} = \mathbf{S}\boldsymbol{x}, \tag{16}$$

where this exosystem is stable, in sense of Layapunov, forward and backward in time, i.e., both (16) and

$$\dot{\boldsymbol{x}} = -\mathbf{S}\boldsymbol{x} \tag{17}$$

are stable in the sense of Lyapunov. An Illustrative example of such system is a ship motion with a single frequency that results in

$$\mathbf{S} = \begin{bmatrix} 0 & \alpha \\ -\alpha & 0 \end{bmatrix}, \tag{18}$$

where α is the unknown to be estimated. In this case, $x = (x_1, x_2)$ and the mapping ℓ is chosen as

$$\ell(x) := x_1/x_2, \tag{19}$$

with the domain $\mathbb{R} \times (\mathbb{R} - \{0\})$. The mapping $\psi_{\boldsymbol{x}}(\alpha)$ is then given by

$$\psi_{\boldsymbol{x}}(\alpha) = \alpha(1 + (\frac{x_1}{x_2})^2) \tag{20}$$

that verifies the second condition, i.e., $\alpha_1(1 + (\frac{x_1}{x_2})^2) > \alpha_2(1 + (\frac{x_1}{x_2})^2)$, $\forall \alpha_1 > \alpha_2$ and $\alpha_1, \alpha_2 \in \mathbb{R}$ and $\forall x \in \Omega$. Thus, the frequency estimator will be in the form

$$\begin{aligned} \dot{\hat{z}} &= -(\hat{z} + \frac{x_1}{x_2})(1 + (\frac{x_1}{x_2})^2) \\ \hat{\alpha} &= \hat{z} + \frac{x_1}{x_2}. \end{aligned} \tag{21}$$

To prove the convergence of the estimates, we define

$$z := \hat{\alpha} - \alpha \tag{22}$$

and prove that z converges to zero as $t \to \infty$. Substituting $\hat{\alpha}$ from (21) we get

$$z = \hat{z} - \alpha + \ell(x), \tag{23}$$

which gives

$$\dot{z} = \dot{\hat{\alpha}} - \frac{\partial \ell}{\partial x}\dot{\boldsymbol{x}}, \tag{24}$$

assuming $\dot{\alpha} = 0$. This assumption sounds restrictive in the first look. However, designing an estimator with high convergence speed will allow us to use the estimator for systems, in which the unknown parameter changes are slow relative to the system states. In order to prove the asymptotic stability of (24), we introduce the Lyapunov function $V(z) = \frac{1}{2}z^2$. Thus, we should show that $\dot{V}(z) = z\dot{z}$ is a negative definite function. Using, (16), (20), and (21) in (24) gives

$$\begin{aligned} \dot{z} &= -\hat{\alpha}(1 + (\frac{x_1}{x_2})^2) + \alpha(1 + (\frac{x_1}{x_2})^2) \\ &= -(\hat{\alpha} - \alpha)(1 + (\frac{x_1}{x_2})^2), \end{aligned} \tag{25}$$

which indicates that

$$z\dot{z} = -(\hat{\alpha} - \alpha)^2(1 + (\frac{x_1}{x_2})^2) \tag{26}$$

is a negative definite function.

4. EXPERIMENT RESULTS

The designed methods in Section 2 and Section 3 are implemented in the hardware shown in Fig. 5. The core components of AHRS hardware are ARM chip and MEMS sensors, whose small size and low price make them the ideal components for AHRS of MSTA.

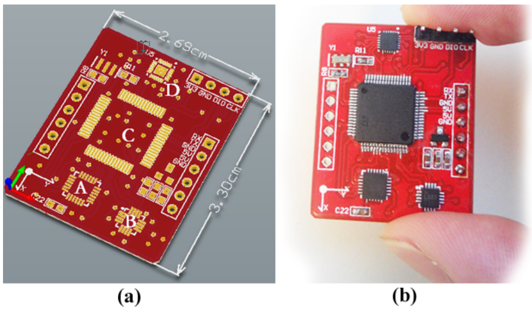

Fig. 5. (a) PCB of AHRS and (b) Appearance of fabricated AHRS (Own pictures).

The Printed Circuit Board (PCB) of AHRS is depicted in Fig. 5(a). To decrease the size of AHRS, this PCB is designed to be in 4 layers. As shown in Fig. 5, a gyroscope and accelerometer sensor (MPU-6000), a magnetometer sensor (HMC5883L), and a microprocessor (ARM Cortex-M4 with 168MHz) are used in the assembly of the small-size AHRS.

In order to decrease the time needed for reading sensor data, a high-speed data bus, SPI, is applied to access data of gyroscope. The transmission speed of SPI can reach 20Mbps, which is much faster than I2C serial communication, whose speed can only be 100Kbps in standard mode or 400Kbps in fast mode.

The cycle frequency of designed AHRS is 500Hz and running results are compared to a high-precision commercial Inertial Measurement Unit (IMU) which is used as attitude reference and is mounted with designed AHRS, as shown in Fig. 6.

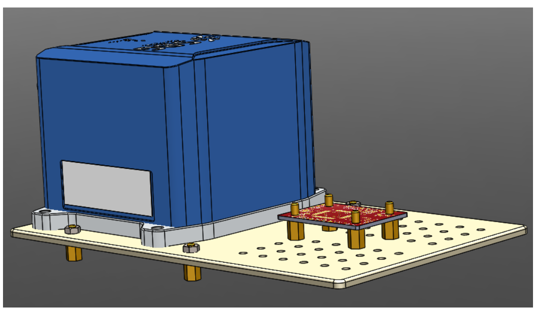

Fig. 6. High-precision commercial IMU is mounted with designed AHRS (Own pictures).

The commercial IMU runs an enhanced on-board Extended Kalman Filter (EKF) to fuse in real-time inertial data with internal GPS information with output data rate of 200Hz. Besides outputting attitude data, it can also output data about position, velicity and heave. With the use of internal dual GPS, its measurement precision of roll, pitch and yaw can reach 0.05deg. Its running picture is shown in Figure 7.

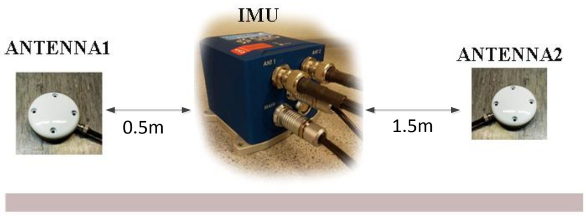

Fig. 7. High precision commercial IMU with two GPS antennas (Own pictures).

For optimal performance, dual GPS antennas are used with this commercial IMU. The primary GPS antenna is the one used for position computation. The secondary GPS antenna (also called sometimes the rover) should be placed in front of the primary antenna and is only used for true heading measurement.That is, magnetometer is not used in this IMU to calibrate the yaw error from gyro integration. Only through the use of the dual GPS antenna with the IMU unit can the yaw precision of 0.05deg be obtained for the reference IMU system.

To facilitate the process from algorithm design to hardware implementation, the code generation tool in Matlab/Simulink is used. In fact, this design paradigm is called Model-Based Design, through which C code for embedded deployment is automatically generated, and code test and system verification are carried out within Matlab/Simulink environment. Using Model-Based Design, the time needed for making product prototype is greatly reduced and the introduction of manually coded errors is also avoided.

The automatically generated C code uses "double" data type, which should be changed to "float" data type. By doing this, the computation burden of generated C code can be greatly reduced. For example, total time consumption of Gauss-Newton method and Kalman filter is reduced to be 310us from 6.08ms by using "float" data type.

The results of attitude estimation are compared with that of commercial IMU.

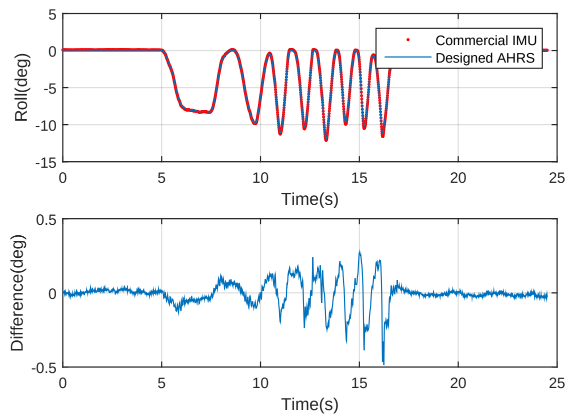

Fig. 8. Comparison of roll between commercial IMU and designed AHRS.

In Fig. 8, the difference of roll between high-precision commercial IMU and designed AHRS is within 0.2deg during low rotation speed (8deg/s) and is within 0.5deg during relatively high rotation speed (25deg/s). The error of roll is very little during static stage and is within 0.1deg.

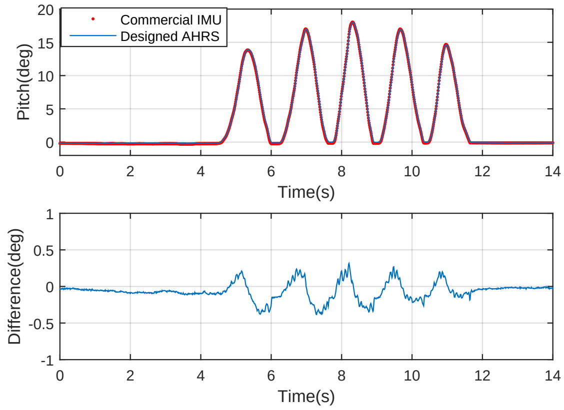

Fig. 9. Comparison of pitch between commercial IMU and designed AHRS.

In Fig. 9, the difference of pitch between high-precision commercial IMU and designed AHRS is within 0.1deg during static stage and is within 0.4deg during dynamic rotation stage (20deg/s).

The wave frequency, f_w, is in the range $0.05Hz < f_w < 0.2Hz$. The rotation frequency of AHRS, f_a, in Fig. 8 and Fig. 9 is about $0.5Hz$, which is fast enough for application in MSTA.

5. CONCLUSION

An adaptive AHRS for measuring the roll, pitch, and yaw of MSTA is developed in this paper. To increase the cycle frequency of attitude estimator, many methods are used, such as using high-speed data bus to read sensor data, applying constant gain matrix in Kalman filter and using float data type in code generation. To make designed AHRS have the same estimation precision under different working environments, an I&I frequency estimator is designed for estimating the rotation frequency which is then used to adjust the gain matrix in Kalman filter. The hardwares, used for running designed algorithms, are introduced, and the running results are compared with a high-precision commercial IMU to validate the usefulness of designed algorithms. The experimental results showed that the attitude estimates are within ± 0.5 deg with respect to the output of a high precision commercial IMU.

The future works would be focused on improving the performance of designed AHRS in the environment where there are external acceleration disturbance and vibration. This is the typical working environment of MSTA, and acceleration disturbance would seriously affect the work of accelerometer.

ACKNOWLEDGEMENTS

Authors would like to thanks Innovation Fund Denmark for financial support. Thanks also goes to SpaceCom A/S for providing assistance with hardware construction.

REFERENCES

Chan, A.L., Tan, S.L., and Kwek, C.L. (2011). Sensor data fusion for attitude stabilization in a low cost quadrotor system. In *Consumer Electronics (ISCE), 2011 IEEE 15th International Symposium on*, 34–39.

Comotti, D. (2011). Orientation estimation based on gauss-newton method and implementation of a quaternion complementary filter.

Comotti, D., Ermidoro, M., Galizzi, M., and Vitali, A. (2013). Development of a wireless low-power multi-sensor network for motion tracking applications. In *Body Sensor Networks (BSN), 2013 IEEE International Conference on*, 1–6.

Fossen, T.I. (2011). *Handbook of Marine Craft Hydrodynamics and Motion Control*. Wiley.

Hu, Y., Yan, Y., Liang, J., and Wang, L. (2013). A miniature, low-cost mems ahrs with application to posture control of robotic fish. 1392 – 1395. Minneapolis, MN, United states.

Liu, X., Ortega, R., Su, H., and Chu, J. (2009). Identification of nonlinearly parameterized nonlinear models: application to mass balance systems. In *Conference on Decision and Control held jointly with the 28th Chinese Control Conference, CDC/CCC*, 4682 –4685.

Liu, X., Ortega, R., Su, H., and Chu, J. (2010). Immersion and invariance adaptive control of nonlinearly parameterized nonlinear systems. *Automatic Control, IEEE Transactions on*, 55(9), 2209 –2214.

Madgwick, S., Harrison, A., and Vaidyanathan, R. (2011). Estimation of imu and marg orientation using a gradient descent algorithm. In *Rehabilitation Robotics (ICORR), 2011 IEEE International Conference on*, 1–7.

Ming, A., Yamaoka, T., Kida, T., Kanamori, C., and Satoh, M.I. (2005). Accuracy improvement of ship mounted tracking antenna for satellite communications. In *Mechatronics and Automation, 2005 IEEE International Conference*, volume 3, 1369–1374 Vol. 3.

Ryan, M. and Miller, G. (2010). Mems based ahrs with adaptive bias estimation for high performance rate sensor replacement. In *Position Location and Navigation Symposium (PLANS), 2010 IEEE/ION*, 214–220.

Soltani, M., Izadi-Zamanabadi, R., and Wisniewski, R. (2011). Reliable control of ship-mounted satellite tracking antenna. *Control Systems Technology, IEEE Transactions on*, 19(1), 221–228.

Soltani, M. (2008). *Fault Diagnosis and Fault Tolerant Control of A Ship-mounted Satellite Tracking Antenna*. Phd thesis.

Soltani, S., Zamanabadi, R., and Wisniewski, R. (2008). Robust fdi for a ship-mounted satellite tracking antenna: A nonlinear approach. In *Control Applications, 2008. CCA 2008. IEEE International Conference on*, 757–762.

Tseng, H. and Teo, D. (1998). Ship-mounted satellite tracking antenna with fuzzy logic control. *Aerospace and Electronic Systems, IEEE Transactions on*, 34(2), 639–645.

Wang, M., Yang, Y., Hatch, R., and Zhang, Y. (2004). Adaptive filter for a miniature mems based attitude and heading reference system. In *Position Location and Navigation Symposium, 2004. PLANS 2004*, 193–200.